Erosion-initiated stromatolite and thrombolite formation in a present-day coastal sabkha setting

Andreas Paul [1], Stephen W. Lokier [1,2,*], Angela Sherry [3,4], Luiza Lessa Andrade [3], Wesley M. Court [1], Cees van der Land [3], Kirsten E. Dutton [3], Ian M. Head [3]

[1] Formerly: Department of Geosciences, The Petroleum Institute, Khalifa University of Science & Technology, P.O. Box 2533, Abu Dhabi, United Arab Emirates.

[2] School of Ocean Sciences, Bangor University, Bangor, Gwynedd, LL57 2DG, United Kingdom

[3] School of Natural and Environmental Sciences, Newcastle University, Newcastle upon Tyne, NE1 7RU, United Kingdom.

[4] Department of Applied Sciences, Northumbria University, United Kingdom.

* Corresponding author, e-mail: s.lokier@bangor.ac.uk

ABSTRACT

Laminated microbial mats and microbialites have been documented from a variety of coastal marine environments. This study aims to provide the first detailed descriptions of intertidal pools, along with their hosted thrombolite and stromatolite structures, from Abu Dhabi, and to propose a model for their formation and evolution. We propose that the development of pools within the upper intertidal zone was initiated by localised erosion of the laminated microbial mats during high energy events. The removal of the protective mats permitted erosion of the underlying unconsolidated sediment to produce erosional scours that continued to develop to produce the pools observed today. The margins of the newly-created submerged environment were colonised by a cyanobacteria dominated microbial community. The precipitation of aragonite cement, associated with the cyanobacteria, stabilised the pool walls and cemented the microbial communities to form stromatolitic and thrombolitic fabrics. Syndepositional cementation was further enhanced by the precipitation of marine cements as a result of evaporation-driven Ca^{2+} and Mg^{2+} supersaturation. Erosion behind and below the cemented pool wall eventually resulted in rim-collapse and the formation of the observed pool margin parallel thrombolite bands. Successive generations of lithification and erosion increased the area of the pool with the earliest thrombolites eroding and becoming increasingly isolated. In summary, the resultant microbialites developed through the complex interplay of erosion, abiotic early lithification and microbially-mediated processes and represent a continuum between unlithified laminated microbial mats and domal microbialites. These features are most likely produced during a sea level scenario of stillstand or transgression, and, as such, may be useful as a diagnostic tool to elucidate the onset of transgression. The newly proposed model for stromatolite formation has significant implications for the recognition and interpretation of similar structures observed in the fossil record.

KEYWORDS

sabkha, erosion, stromatolite, thrombolite, microbialite, lithification

INTRODUCTION

Stromatolites are laminated benthic microbial deposits (Riding, 1999) formed through lithification processes mediated or controlled by microbial communities of archaea, bacteria and/or diatoms (Dupraz et al., 2011). Stromatolites appear throughout much of the stratigraphic record, occurring from the Early Archean (Allwood et al., 2006) to the Recent with different organisms taking on the role of bioconstructors at different times. Extant stromatolites have been documented from a variety of coastal marine settings, the best well-known being the structures observed at Hamlin Pool, Shark Bay, Western Australia (Golubic, 1985; Jahnert and Collins, 2013; Logan, 1961; Reid et al., 2003) and from the Bahamas (Andres and Reid, 2006; Bowlin et al., 2012; Monty, 1972; Stolz et al., 2009). Microbial mats, thrombolites and stromatolites have also been described from numerous other coastal settings, including Lagoa Vermelha, Brazil (Vasconcelos et al., 2006), Cayo Coco lagoon, Cuba (Bouton et al., 2016), the Caicos Platform (Trembath-Reichert et al., 2016) and the coastal sabkhas of the Persian Gulf (Brauchli et al., 2016; Court et al., 2017; Evans, 1966; Kendall and Skipwith, 1968; Lokier et al., 2017).

Despite the long stratigraphic history and significant geographical range of these biologically-generated sedimentary structures, models for their mode of formation have been surprisingly limited to studies of Recent examples from only a limited number of depositional settings. Such a paucity of studies is even more surprising when one considers that in many ‘stressed’ environments the microbial communities associated with stromatolite and thrombolite formation were the dominant and, often, only biota interacting with sediments at the time of deposition. Succinctly, while stromatolites and thrombolites have a significant potential as a tool for paleoenvironmental interpretation, such utility requires that their mode of formation is considered from a range of depositional settings and potential distinguishing characteristics are identified.

The stromatolite communities living at the southern shoreline of the Persian/Arabian Gulf (hereafter referred to as the Gulf) provide an ideal site to study stromatolite formation in a previously-undescribed coastal environment. The presence of thrombolitic, hemispheroid microbial mats and stromatolite-like features from the coastal sabkha of Abu Dhabi has been noted (Kendall and Skipwith, 1968), yet, to date, no detailed description and interpretation of these features has been made. This study aims to provide the first detailed descriptions of the thrombolite and stromatolite structures at the seaward margin of the coastal sabkha complex of Abu Dhabi. The study does not aim to provide a detailed analysis of the composition of the microbial communities forming the stromatolites. Rather, the focus of the study is to describe and explain the morphology of the resultant stromatolite structures within the context of the environmental factors observed in the depositional setting and to consider their mode-of formation in the context of how these observations may be employed to constrain paleoenvironmental interpretations of similar features from the depositional record.

STUDY AREA

The study area is located at the southern shore of the Gulf, approximately 40 km to the southwest of Abu Dhabi City (Fig. 1A, B). The Gulf is a shallow microtidal sea with an average water depth of 35 m and a tidal range of 1.5 m in open-marine areas and less than 1 m in lagoons. At the Abu Dhabi coastline, temperatures range between 7 °C at night during the winter and exceed 50 °C during summer months (Lokier, 2012). Average annual rainfall is 72 mm, predominantly occurring as brief, heavy, downpours during winter months (Raafat, 2007). Arid conditions result in evaporation (2.75 m per year) far exceeding precipitation (Bottomley, 1996).

The southeast region of the Gulf comprises a low-angle, north-sloping, ramp geometry that was rapidly flooded as post-glacial eustatic sea level rise transgressed an aeolian dune system resulting in a transition from aeolian-siliciclastic to marine-carbonate dominated deposition (Evans et al., 1969; Lambeck, 1996; Lokier and Steuber, 2008). A short-lived still stand, between 7,100 - 6,890 cal yrs BP (Lokier et al., 2015), facilitated the development of coastal sabkhas prior to renewed transgression with the onset of the Middle Holocene Atlantic stage. The subsequent relative sea level fall and stillstand resulted in the development of a strongly progradational geometry throughout the Middle to Late Holocene (Lokier and Steuber, 2008; Lokier et al., 2015).

From seaward to landward, the surface facies of the modern sabkha (Fig. 1C) are characterised by peloidal carbonate sands in the lower and middle intertidal zone (lagoon), a coast-parallel microbial mat belt in the upper intertidal zone, and evaporite precipitates in the supratidal zone (Evans et al., 1969; Kendall and Skipwith, 1969). The spatial occurrence of these facies belts is controlled by the local angle of slope which governs the duration of tidal flooding (Court et al., 2017). The microbial mat belt varies in width between 150 to 800 m and is classified (Court et al., 2017) based on surface morphologies resulting from the duration of inundation.

METHODOLOGY

Google Earth satellite imagery was used to identify areas of the intertidal zone where channels and pools were present. A field reconnaissance campaign, in January 2016, identified an area containing an ephemeral ponds network, tidal channels and the intertidal pool that is the focus of this study. The morphology of the pool was mapped using a Garmin GPSmap 78 device; the data was subsequently imported and processed in Quantum GIS 2.18. Microbial, including stromatolite and, thrombolites features, and other sedimentary and biological characteristics of the pool were documented in detail. Monitoring and sampling visits were regularly made between January 2016 and May 2017 with any changes to the morphology of the pool or the associated features being documented in detail. Three specimens of microbialite from the pool margin and one specimen of thrombolite from the pool centre were recovered and subsequently stored in seawater in plastic containers.

A weather station (WS-GP1, Delta-T Devices), 3 km landwards from the study site (Fig. 1C) recorded air temperature, air humidity, wind direction, wind speed, and precipitation at a height of 1.2 m between April 2016 and July 2017. Battery failure resulted in data loss between February and March 2017. Barometric pressure and temperature data were recorded at 30 minute intervals between February 2016 and June 2017 using a Baro-Diver barometric logger (Van Essen Instruments) sited approximately 2 km to the east of the weather station (Fig. 1C). Data analysis and visualisation were conducted in the statistical computing language R, in the programming language Python version 2.7.10 and in PAST version 3.15.

The physico-chemical characteristics of the water in the studied pool were measured using an Ultrameter II 6PFC device (Myron L Company) to record temperature, conductivity, total dissolved solids (TDS), oxidation-reduction potential (ORP), resistivity and pH. Very high dissolved solid load resulted in resistivity measurements that exceeded instrument parameters and, thus, were not used for interpretations. Salinity was measured using a Brix-type refractometer with automatic temperature compensation. The water level in the studied pond was monitored between February to October 2016 using a CTD-diver water level logger (Van Essen Instruments) installed 5 cm above the pool base. Water level was recorded as pressure in mbar, with a barometric conversion applied by subtracting barometric pressure from the water level pressure, under the assumption that 1 mbar = 1 cm of H_2O.

The microbialite structures were investigated at the micro-scale using a Quanta 200 (FEI) scanning electron microscope (SEM), located at The Petroleum Institute of Khalifa University of Science & Technology. One smaple was selected from which representative sections were broken off, cleaned with compressed air, mounted on metal stubs, and coated with a palladium/gold mixture. The energy-dispersive X-ray spectroscopy mode (EDX) of the SEM was used to semi-quantitatively characterise element compositions of specific features. Samples were also prepared for analysis under the low-vacuum conditions of the environmental SEM mode. These samples rapidly dehydrated and became charged, it was therefore decided to focus on careful sample preparation and application of the conventional SEM mode.

Petrographic thin sections were prepared from three microbialite specimens, including the specimen that was investigated in the SEM. The sample were cut using a diamond rock saw and subsequently left to dry in the laboratory for 24 hours. Each sample was then impregnated with blue resin to enhance the visibility of pore space under the optical microscope.

DNA was extracted from samples of polygonal microbial mat, using a FastDNA SPIN kit for soil (Q-BIOgene, Cambridge, UK), according to the manufacturer's instructions. DNA sequencing was performed on a MiSeq Personal Sequencer (Illumina) at the NUomics Facility (Northumbria University, Newcastle, UK). Gene amplicon libraries (16S rRNA) were prepared, including PCR amplification, purification of amplicons and quantification procedures, according to the procedures of Kozich et al., 2013. Aliquots of purified amplicons were sequenced to produce 2 x 250 bp paired-end reads with v2 chemistry. Raw sequencing reads were analysed using QIIME2 (Bolyen et al., 2019), with Amplicon Sequence Variants (ASVs) determined using Divisive Amplicon Denoising Algorithm (DADA2, Callahan et al., 2016). Taxonomic classification of representative ASV sequences was performed using the Naïve Bayesian classifier (Bokulich et al., 2018). The relative abundance of ASVs was calculated by taking the sum of the reads for individual ASV abundances and dividing by the total number of reads for all ASVs within a sample and multiplying by 100.

RESULTS

Environmental data

Air temperatures recorded by the weather station ranged between 8.4 °C and 48.9 °C; air temperatures recorded by the barometric logger ranged between 8.9 °C and 53.7 °C (Fig. 2A). The highest temperatures were recorded during July and August, while the lowest temperatures were recorded during February. Total precipitation over the measurement period amounted to 7.6 mm, mainly resulting from torrential rainfall events in January and February 2017 (Fig. 2A). March 2017 experienced heavy rainfall, but, as previously mentioned, this data was not recorded by the weather station due to a battery failure. Therefore, the rainfall data represent a minimum value for the measurement interval. The primary wind direction throughout the recording period was from the north-west, with subordinate winds from the south (Fig. 2C). Wind speed varied between 0.3 - 15.4 m/s with a mean of 3.7 m/s (Fig. 2C, D).

Water temperatures in the pool ranged between 11.7 °C and 46.8 °C during the measurement period (Fig. 2B). The lowest water temperatures were recorded in February while the highest water temperatures were recorded in August. Salinity ranged between 75.0 ‰ to 93.0 ‰, accompanied by pH values between 7.3 to 8.1. Of the remaining physico-chemical parameters, conductivity ranged between 100.0 - 118.7 mS/cm, TDS ranged between 75.0 - 91.26 parts per thousand (ppt), and ORP values ranged from 79 mV to 100 mV. The tidal regime in the studied pool was semi-diurnal micro-tidal, with a water depth ranging from a minimum of 19 cm when the pool was emergent up to a maximum of 109 cm during an unusually high tide (Fig. 2B).

Pool morphology and hydrological regime

The studied intertidal pool is located at the seaward margin of the polygonal microbial mat zone (Fig. 1C). The pool is broadly U-shaped and hydrologically open at its seaward and landward sides (Fig. 3A, B). The seaward opening of the pool corresponds to the landward termination of a tidal channel that extends into the lower intertidal and subtidal zones. The landward opening to the pool is defined by a narrow, well-lithified, sill that provides a connection to an elevated landward ephemeral pond system (Fig. 4). Ebb tide water continues to flow into the pool over this sill even whilst the next flood tide is recharging the pool via the tidal channel. The pool exhibits a perimeter of approximately 80 m and an area of approximately 250 m^2. The height difference between the cemented floor of the pool and its upper rim ranges between 20 to 30 cm. The floor of the pool is always submerged, this is in stark contrast to the elevated surrounding areas of microbial mat that experience daily cycles of exposure and inundation.

Macro-scale sedimentary and biological features

The general stratigraphy in the area of the pool (Fig. 3C) consists of Pleistocene to Early Holocene aeolian mixed siliciclastic-carbonate sands, overlain by a shallow-marine transgressive carbonate hardground of mid-Holocene age (Ge et al.; Lokier and Steuber, 2009; Paul and Lokier, 2017), followed by an overlying unconsolidated, to lightly-cemented, bioclastic rudstone. This sequence is terminated by laminated microbial mats with a polygonal surface architecture. At the pool-floor, the hardground is locally exposed or is covered by an organic ooze that increases in thickness (up to 7 cm) landward (Figs 3 and 5). Accumulations of spongy, unlithified, mobile, gravel-sized grains are observed throughout the pool. These grains vary in colour and typically accumulate in small troughs and in the lee of thrombolite patches and bands. The grains vary in diameter between 5-10 mm and are irregularly shaped (Fig. 6A). The grains contain sub-mm scale inclusions of bioclastic grains including benthic foraminifera (Fig. 6B-D).

Clotted microbial (thrombolite) fabrics are distributed within the pool as isolated domes or discontinuous dm to m-long bands that are typically oriented parallel to the pool margin (Fig. 7A). The thrombolite domes typically measure between 5-20 cm in width, and exhibit relief above the hardground of between 10-25 cm. The structures are coloured brown to dark brown, and are characterised by a spongy consistency that reflects a dominantly cyanobacteria composition. Cyanobacteria were detected throughout polygonal mats in the area ($\sum$ relative abundance; 8.5% ±2.1), with different morphologies including coccoid (*Halothece*, *Gleocapsa*) and filamentous (*Coleofasciculus*, *Lyngbya*, *Phormidium*) forms. A mm-thick cover of bioclastic grains is locally present at the upper surface of the thrombolites (Fig. 7B). Marine brown and green algae grow at the outer margins of individual thrombolites, defining the minimum water depth within the pool. Internally, the domal structures comprise two distinct intervals (Fig. 3C). The upper interval is a thrombolite, exhibiting crude laminations corresponding to different colours of microbial communities interlayered with bioclasts (Fig. 8A). The lower layer is a ~10 cm thick laminated stromatolite that is attached to the underlying hardground (Fig. 8B). The margins of the pool exhibit the same vertical facies distribution as the thrombolite domes and bands but are locally undercut by up to 10 cm (Figs 3 and 9).

Moving away from the pool, into the adjacent microbial mats, the lithified cyanobacterial communities of the pool margin transition over decimetres into an unlithified finely-laminated and polygonal microbial mat dominated by filamentous cyanobacteria (Fig. 10). Elongate scours in excess of 1 m long are distributed throughout the polygonal microbial mat zone (Fig. 11). The scours are oriented perpendicular to the shoreline, are shallowest at their seaward end and gradually deepen landward. The scours host a variety of microbial communities that closely resemble the organic ooze observed in the pool.

Micro-facies and cement fabrics

The pool margin microbialites contain abundant lithoclasts, bioclasts, peloids and coated grains (Fig. 12A) surrounded by pervasive microbial extracellular polymeric substance (EPS) (Figs 13A, B). The skeletal assemblage observed within the microbialites is dominated by benthic foraminifera (primarily peneropolids) and ostracods with subordinate bivalves. Skeletal grains are typically whole with little evidence of abrasion or breakage (Fig. 12A). SEM observations reveal the presence of cyanobacteria tubes and filaments within the EPS (Fig. 13 B, E). Primary microbial laminae are difficult to discern in thin section, occurring as discontinuous degraded organic seams that could be easily confused with dissolution seams (Fig. 12E, F).

Grains are coated by an isopachous fringing acicular (Sandberg et al., 1985) aragonite cement with fibrous needles oriented perpendicular to grain surfaces (Figs 12B-D). The aragonite needles exhibit pointed crystal terminations, have a length of 16-185 μm with a width of 3-5 μm (axial ratio typically >22). Rare dolomite cements occur as isolated rhombs between 3-6 μm and more-massive clusters of slightly coarser (up to 8 μm) equant euhedral crystals (Fig. 13C, D). These dolomite crystals are enclosed in microbial EPS and acicular aragonite. Semi-quantitative EDX elemental analysis of the dolomite crystals yield an Mg content of between approximately 20-40% compared to significantly lower values (~14%) in the surrounding matrix (Fig. 13 C, D).

Primary interparticle porosity has been largely occluded by the pervasive precipitation of the aragonite cement phase that has cemented grains and significantly restricted pore throats (Fig. 12C, D). Secondary, yet syndepositional, mouldic porosity after bioclasts (Fig. 12B), has also been partially to completely occluded by the precipitation of the aragonite cement phase.

INTERPRETATION AND DISCUSSION

On the basis of field and laboratory observations, it is here proposed that the formation of the intertidal pools and the subsequent genesis of the hosted stromatolite and thrombolite microbial fabrics are genetically related.

Formation of intertidal pools and associated microbialites

As has been previously documented, the development of significant modern-day microbial mat communities requires stressed environmental conditions that prevent competition from macroalgae and other eukaryotic organisms (Bouton et al., 2016; Bowlin et al., 2012; Suosaari et al., 2016b). In the case of the Abu Dhabi sabkha, these conditions are met in the uppermost intertidal zone where diurnal flooding is sufficient to maintain microbial growth, yet exposure inhibits competition. Under such conditions, laminated, unlithified, microbial communities are able to thrive.

Pool formation is initiated where a high energy event, such as a storm surge or high tide, removes the protective binding microbial mat and exposes the underlying unconsolidated sediment (Fig. 11A). Under the prevailing relatively low-energy conditions of the Abu Dhabi sabkha, such events are relatively rare and of limited duration, thus normally allowing recolonisation of the sediment surface by a new generation of microbial mat and the effective ‘healing’ of the protective binding layer. However, prolonged episodes of high energy, or multiple high energy events over a short time interval, will erode the unprotected sediment to produce an erosional scour that may extend to the depth of the underlying lithified hardground (Figs 11B, 14B). Initially, the unprotected vertical walls of the pond are susceptible to continued erosion, thereby facilitating lateral growth of the pool.

With a return to quiescent conditions, the newly formed pool walls (Fig. 11B) provide a submerged substrate for the development of cyanobacteria dominated microbial communities that overgrow the exposed truncated surface of the laminated microbial mats (Figs 9, 10) and promote aragonite precipitation (Figs 12, 13). Lithification stabilises both the underlying laminated microbial mat substrate, producing stromatolite fabrics, and the clotted textures to form a thrombolitic fabric (Fig. 14C). Increasing lithification stabilises the pool walls and inhibits erosion during subsequent high energy events.

Microtidal flooding cycles ensure regular marine inundation of both the pool and surrounding microbial mats by seawater that is oversaturated with respect to Ca^{2+} and Mg^{2+} (Paul and Lokier, 2017; Shinn, 1969; Wood and Sanford, 2002). Ebb tide surface flow is concentrated into tidal channels that rapidly drain much of the upper intertidal zone. High evaporation rates and shallow sub-surface bacterial sulphate reduction (Lokier and Steuber, 2008) further increase the concentrations of major ions in ponded surface and shallow subsurface waters. Localised dissolution of aragonite allochems (Fig. 12B) occurs where the pH of the pore-water is reduced by the oxidisation of hydrogen sulphide (Jordan et al., 2015). These highly saline, Ca^{2+} and Mg^{2+} oversaturated pore-waters flow seawards in the shallow subsurface until they intercept the pool margin and discharge into the pool, further promoting the precipitation of aragonite cements (Fig. 14C).

Over time, the pool walls become increasingly lithified through the continued precipitation of aragonite cements. During high tides, waves breaking at the pool 'shore' will erode the unlithified microbial mats immediately behind the wave-resistant cemented pool margin (Figs 3, 14C). Simultaneously, currents will erode the unlithified basal rudstone to undercut the pool wall (Fig. 9) and further destabilise the edge of the pool. This process will eventually result in the detachment of a section of the cemented microbial thrombolites and stromatolites which will founder onto the exposed hardground at the pool floor to create detached sub-aqueous margin-parallel thrombolite bands (Figs 3, 7A, 14D). The submerged thrombolite bands will continue to grow and precipitate aragonite cements within their clotted fabric (Fig. 13). High energy events, such as storm surges, will detach and remove sections of the thrombolite bands. Erosion will decrease over time as the precipitation of early marine aragonite (Lokier and Steuber, 2008; Paul and Lokier, 2017) cements the thrombolite to the underlying hardground and stabilises the structure (Fig. 14E).

The freshly-exposed pool margin is now subject to renewed microbial colonisation and associated aragonite precipitation and the process is repeated with the genesis of a new generation of margin-parallel thrombolite band (Fig. 14F). With repeated cycles, this process will result in significant lateral expansion of the pool, possibly resulting in coalescence with any adjacent pools. Over time, the earlier thrombolites will become increasingly isolated (Fig. 3) and may be subjected to undercutting to produce the distinctive dome-shaped morphology with clotted thrombolitic fabrics sitting atop laminated stromatolites (Figs 7B, 8, 14F). These thrombolite domes superficially resemble the 'isolated patch' macrofabrics described from the Cayo Coco Lagoon, Cuba (Bouton et al., 2016). However, the Cayo Coco structures appear to be entirely thrombolitic in nature, lacking either a laminated stromatolite component or a relationship with an underlying hardground.

The accumulations of unlithified, spongy, microbial gravel-grade grains at the pool floor (Figs 6, 7A) are comprised of cyanobacteria and EPS forming a clotted microbial fabric akin to that of the thrombolites. These soft grains are inferred to have been sourced from the thrombolite domes or pool margin thrombolite bands either through erosion or via exfoliation due to high rates of microbial production. Once disarticulated, the low-density grains are particularly susceptible to reworking and concentration in the lee of thrombolites and in bathymetric lows. Where a significant amount of carbonate material is bound within these grains, it is possible that they may be preserved in, and recognised from, the geologic record as large aggregate grains with a clotted matrix (Gerdes et al., 1994). In more-open areas of the pond, agitation of the microbial grains, by wave and current action, will result in abrasion and disarticulation to generate the microbial ooze that covers much of the pool floor.

The rare small, EPS-hosted, dolomite crystals observed in the pool-margin stromatolites are consistent with a microbially-mediated origin as proposed previously (Bontognali et al., 2010). Under this model, the fluctuating hypersaline conditions of the sabkha environment result in the EPS generating carboxyl functional groups that overcome the kinetic barrier to the low temperature incorporation of Mg into carbonate minerals (Bontognali et al., 2014; Petrash et al., 2017). These clusters of dolomite crystals bare a remarkably similarity, in terms of size, distribution and association with biofilms, to those previously documented from the Lower Messinian of Sicily (Oliveri et al., 2010).

The well-lithified nature of the sill separating the pool from the landward ephemeral ponds is inferred to result from a combination of microbially-mediated aragonite precipitation enhanced by degassing-related precipitation as the solubility product of the outflowing water is lowered as it cascades over the sill margin. This process is similar to the precipitation of carbonates at travertine terraces and tufas (Fig. 15; Gandin and Capezzuoli, 2014; Özkul et al., 2014).

Microbialite formation in a sea level context

The formation of the pools and their associated microbial communities is inferred to preferentially occur under prevailing conditions of relative sea level stillstand or, more likely, under the increased hydrodynamic conditions associated with relative sea level rise. The present-day rate of eustatic sea level rise (3.2 mm yr^{-1}) (Church et al., 2013) has been previously documented as resulting in significant shoreline retreat (up to 29 m yr^{-1}) and associated hydrodynamic energy increase at the Abu Dhabi coastline (Lokier et al., 2018). Under such a transgressive (flooding) scenario it is expected that we shall observe an increase in the frequency and amount of erosion of the unlithified upper intertidal microbial mats and, consequently, the increased initiation and development of pools with their associated stromatolite and thrombolite fabrics. However, under conditions where the rate of relative sea level rise is ‘too rapid’, the associated increase in energy at the shoreline may result in dynamic coastline retreat at a rate that exceeds the ability of the microbial systems to re-establish and ‘track’ retrogradation.

From an environmental perspective, as the rate of present-day eustatic sea level rise continues to increase (Church et al., 2013), coastal microbial communities will be placed increasingly under threat and should thus be added to the growing list of coastal and shallow-marine ecosystems (Lovelock et al., 2015; Perry et al., 2018; Thorner et al., 2014) that are at risk due to anthropogenic-driven global warming and associated sea level rise.

Microbialite preservation and identification in the fossil record

Under a rising sea level scenario, as observed in the study area today, the preservation potential of the described structures is primarily dependent on the degree of early-lithification and the subsequent rate of burial. As sea level rises, increased hydrodynamic energy easily erodes the uncemented microbial mats and thrombolites, transporting much of the material into the marine system where it is consumed. The likelihood of preservation of unlithified microbial features is further compromised as increased, and more regular, inundation reduces environmental stress in the intertidal and shallow subtidal zone. Such increased flooding opens this niche-environment to colonisation by macro-algae and other eukaryotes that will outcompete and displace the microbial communities. On entering the burial realm, ongoing degradation of the organic component of the unlithified microbial mats and thrombolites will further reduce the potential for preservation and identification within the stratigraphic record (Court et al., 2017; Kenig et al., 1990).

Conversely, cemented stromatolites and thrombolites have a significantly higher prospect of preserving primary depositional fabrics during inundation and subsequent burial and will, thus, have a higher preservation and recognition potential into the stratigraphic record. Where these early-lithified structures remain exposed at the sea floor, or are covered by only a thin veneer of sediment, they will be subject to early-marine cementation, thereby further enhancing the potential of preservation. If exposed at the sea floor, the lithified structures will act as a stable substrate for colonisation by sessile benthic communities, again enhancing the potential of preservation but providing a challenge for identification in the fossil record.

Where ponds and their associated structures have formed during a period of high sea level or falling stage stillstand, the chances of preservation into the fossil record are significantly reduced. During post-stillstand base level fall, unlithified microbial communities are subject to biodegradation and physical erosion. On entering the meteoric realm, lithified microbial structures will be subject to increased dissolution of aragonite cements and allochems. As erosion removes the surrounding unlithified sediments, the increasingly exposed cemented pond margins will lose their support, becoming unstable and subject to increased likelihood of erosion. This process may continue until all of the sediments are eroded to expose the underlying, strongly lithified, transgressive hardground, thereby potentially removing all evidence of the preceding transgressive cycle. Under these circumstances, transgressive sequences will only be preserved into the stratigraphic record where high frequency (4^{th}-5^{th} Order) transgressive cycles occur during a theme of overall, lower order, sea level rise. This scenario will result in repeated transgressive cycles punctuated by stillstands to produce parasequences as observed in the sabkha stratigraphy of the Jurassic Arab Formation (Grötsch et al., 2003).

Under the above-proposed scenarios, preservation of these structures into the geological record is only likely under a rising sea level scenario and where the microbial structures have been lithified. As such, the recognition of these systems from the stratigraphic record offers a potential diagnostic tool to elucidate the onset and, possibly, rate of marine transgression.

The differential preservation potential of lithified and unlithified components together with a limited thickness and laterally isolated morphology of these systems offers many challenges to their observation and interpretation in the geological record. Identification of the system requires recognition of lateral and vertical facies relationships and gross morphologies that is best suited to observation in laterally extensive outcrops. Conclusive identification of these systems from core would be significantly more challenging. A vertical stacking pattern of transgressive hardgrounds succeeded by stromatolites and overlying thrombolites, possibly with encrusting marine benthos, would hint at the presence of these systems. However, these vertical relationships could also be observed under other formational mechanisms, such as those described from Storr's Lake (Dupraz et al., 2013) and Shark Bay (Jahnert and Collins, 2011; Logan et al., 1974), and, without a significant density of cores, it is unlikely that the required knowledge of lateral facies geometries could be achieved from core alone.

CONCLUSIONS

Intertidal pools and associated microbial fabrics were observed and documented from the coastal sabkha of Abu Dhabi. We propose a new, erosion-based, model for the formation of these systems under a scenario of rising relative sea level. Increasing energy at the shoreline results in erosion of protective microbial mats to expose underlying sediments to erosion and initiate pool formation. These newly-formed submerged environments provided an ideal habitat for the pervasive growth of cyanobacteria that promoted the cementation of stromatolite and thrombolite textures thereby significantly increasing the potential for the preservation of these microbial structures. Successive erosional events enlarged the pools and created isolated microbialites with a range of textures.

Although the recognition of these features in the stratigraphic record may be challenging, their association with the onset of transgression makes them a potentially powerful diagnostic tool for constraining the initiation of relative sea level rise.

ACKNOWLEDGEMENTS AND DATA AVAILABILITY

All sample site locations are clearly defined in the manuscript text and figures. If additional sample or other data are required then these can be accessed by contacting the corresponding author. This study was funded by the Petroleum Institute Research Centre (PIRC/ADRIC) through project LTR15003 titled 'Understanding ancient petroleum carbonate systems; carbonate precipitation in Abu Dhabi microbial mats as a modern analogue'. The authors declare no conflict of interest related to this study. Our sincere appreciation goes to Sion Kennaway for general laboratory and field support, to Warren Marilag for preparing the petrographic thin sections, and to Prasanth Thiyagarajan for his assistance with the SEM and EDS analyses. Xin Bixiao and Yuan Peng are thanked for their help during the many long field-days in the sabkha of Abu Dhabi. We thank Tomaso Bontognali, Edoardo Perri and two anonymous reviewers for their very constructive comments. We also acknowledge Associate Editor Alexander Brasier and Chief Editor Peir Pufahl for their helpful comments and guidance through the editorial process.

REFERENCES

Allwood, A.C., Walter, M.R., Kamber, B.S., Marshall, C.P. and Burch, I.W. (2006) Stromatolite reef from the Early Archaean era of Australia. *Nature*, **441,** 714-718.

Andres, M.S. and Reid, P.R. (2006) Growth morphologies of modern marine stromatolites: A case study from Highborne Cay, Bahamas. *Sedimentary Geology*, **185,** 319-328.

Bokulich, N.A., Kaehler, B.D., Rideout, J.R., Dillon, M., Bolyen, E., Knight, R., Huttley, G.A. and Gregory Caporaso, J. (2018) Optimizing taxonomic classification of marker-gene amplicon sequences with QIIME 2's q2-feature-classifier plugin. *Microbiome*, **6,** 90.

Bolyen, E., Rideout, J.R., Dillon, M.R., Bokulich, N.A., Abnet, C.C., Al-Ghalith, G.A., Alexander, H., Alm, E.J., Arumugam, M., Asnicar, F., Bai, Y., Bisanz, J.E., Bittinger, K., Brejnrod, A., Brislawn, C.J., Brown, C.T., Callahan, B.J., Caraballo-Rodríguez, A.M., Chase, J., Cope, E.K., Da Silva, R., Diener, C., Dorrestein, P.C., Douglas, G.M., Durall, D.M., Duvallet, C., Edwardson, C.F., Ernst, M., Estaki, M., Fouquier, J., Gauglitz, J.M., Gibbons, S.M., Gibson, D.L., Gonzalez, A., Gorlick, K., Guo, J., Hillmann, B., Holmes, S., Holste, H., Huttenhower, C., Huttley, G.A., Janssen, S., Jarmusch, A.K., Jiang, L., Kaehler, B.D., Kang, K.B., Keefe, C.R., Keim, P., Kelley, S.T., Knights, D., Koester, I., Kosciolek, T., Kreps, J., Langille, M.G.I., Lee, J., Ley, R., Liu, Y.-X., Loftfield, E., Lozupone, C., Maher, M., Marotz, C., Martin, B.D., McDonald, D., McIver, L.J., Melnik, A.V., Metcalf, J.L., Morgan, S.C., Morton, J.T., Naimey, A.T., Navas-Molina, J.A., Nothias, L.F., Orchanian, S.B., Pearson, T., Peoples, S.L., Petras, D., Preuss, M.L., Pruesse, E., Rasmussen, L.B., Rivers, A., Robeson, M.S., Rosenthal, P., Segata, N., Shaffer, M., Shiffer, A., Sinha, R., Song, S.J., Spear, J.R., Swafford, A.D., Thompson, L.R., Torres, P.J., Trinh, P., Tripathi, A., Turnbaugh, P.J., Ul-Hasan, S., van der Hooft, J.J.J., Vargas, F., Vázquez-Baeza, Y., Vogtmann, E., von Hippel, M., Walters, W., Wan, Y., Wang, M., Warren, J., Weber, K.C., Williamson, C.H.D., Willis, A.D., Xu, Z.Z., Zaneveld, J.R., Zhang, Y., Zhu, Q., Knight, R. and Caporaso, J.G. (2019) Reproducible, interactive, scalable and extensible microbiome data science using QIIME 2. *Nature Biotechnology*, **37,** 852-857.

Bontognali, T.R.R., McKenzie, J.A., Warthmann, R.J. and Vasconcelos, C. (2014) Microbially influenced formation of Mg-calcite and Ca-dolomite in the presence of exopolymeric substances produced by sulphate-reducing bacteria. *Terra Nova*, **26,** 72-77.

Bontognali, T.R.R., Vasconcelos, C., Warthmann, R.J., Bernasconi, S.M., Dupraz, C., Strohmenger, C.J. and McKenzie, A.J. (2010) Dolomite formation within microbial mats in the coastal sabkha of Abu Dhabi (United Arab Emirates). *Sedimentology*, **57,** 824-844.

Bottomley, N. (1996) Recent climate of Abu Dhabi. In: *Desert ecology of Abu Dhabi. A review and recent studies* (Ed P.E. Osborne), pp. 36-49. Pisces, Newbury.

Bouton, A., Vennin, E., Pace, A., Bourillot, R., Dupraz, C., Thomazo, C., Brayard, A., Désaubliaux, G. and Visscher, P.T. (2016) External controls on the distribution, fabrics and mineralization of modern microbial mats in a coastal hypersaline lagoon, Cayo Coco (Cuba). *Sedimentology*, **63,** 972-1016.

Bowlin, E.M., Klaus, J.S., Foster, J.S., Andres, M.S., Custals, L. and Reid, R.P. (2012) Environmental controls on microbial community cycling in modern marine stromatolites. *Sedimentary Geology*, **263–264,** 45-55.

Brauchli, M., McKenzie, J.A., Strohmenger, C.J., Sadooni, F., Vasconcelos, C. and Bontognali, T.R.R. (2016) The importance of microbial mats for dolomite formation in the Dohat Faishakh sabkha, Qatar. *Carbonates and Evaporites*, **31,** 339-345.

Callahan, B.J., McMurdie, P.J., Rosen, M.J., Han, A.W., Johnson, A.J.A. and Holmes, S.P. (2016) DADA2: High-resolution sample inference from Illumina amplicon data. *Nature Methods*, **13,** 581-583.

Church, J.A., Clark, P., U., Cazenave, A., Gregory, J.M., Jevrejeva, S., Levermann, A., Merrifield, M.A., Milne, G., A., Nerem, R.S., Nunn, P.D., Payne, A.J., Pfeffer, W.T., Stammer, D. and Unnikrishnan, A.S. (2013) Sea Level Change. In: *Climate Change 2013: The Physical Science Basis: Working Group I Contribution to the Fifth Assessment Report of the Intergovernmental Panel on Climate Change* (Eds T.F. Stocker, D. Qin, G.-K. Plattner,

M. Tignor, S.K. Allen, J. Boschung, A. Nauels, Y. Xia, V. Bex and P.M. Midgley), pp. 1137-1216. Cambridge University Press, Cambridge, United Kingdom and New York, NY, USA.

Court, W.M., Paul, A. and Lokier, S.W. (2017) The preservation potential of environmentally diagnostic sedimentary structures from a coastal sabkha. *Marine Geology*, **386,** 1-18.

Dupraz, C., Fowler, A., Tobias, C. and Visscher, P.T. (2013) Stromatolitic knobs in Storr's Lake (San Salvador, Bahamas): a model system for formation and alteration of laminae. *Geobiology*, **11,** 527-548.

Dupraz, C., Reid, R.P. and Visscher, P.T. (2011) Microbialites, Modern. In: *Encyclopedia of Geobiology* (Eds J. Reitner and V. Thiel), pp. 617–635. Springer, Netherlands.

Evans, G. (1966) The Recent Sedimentary Facies of the Persian Gulf Region. *Philosophical Transactions of the Royal Society of London. Series A, Mathematical and Physical Sciences*, **259,** 291-298.

Evans, G., Schmidt, V., Bush, P. and Nelson, H. (1969) Stratigraphy and geologic history of the sabkha, Abu Dhabi, Persian Gulf. *Sedimentology*, **12,** 145-159.

Gandin, A. and Capezzuoli, E. (2014) Travertine: Distinctive depositional fabrics of carbonates from thermal spring systems. *Sedimentology*, **61,** 264-290.

Ge, Y., Pederson, C.L., Lokier, S.W., Traas, J.P., Nehrke, G., Neuser, R.D., Goetschl, K.E. and Immenhauser, A. Late Holocene to Recent aragonite-cemented transgressive lag deposits in the Abu Dhabi lagoon and intertidal sabkha. *Sedimentology*, **n/a**.

Gerdes, G., Dunajtschik-Piewak, K., Riege, H., Taher, A.G., Krumbein, W.E. and Reineck, H.-E. (1994) Structural diversity of biogenic carbonate particles in microbial mats. *Sedimentology*, **41,** 1273-1294.

Golubic, S. (1985) Microbial mats and modern stromatolites in Shark Bay, Western Australia. In: *Planetary Ecology* (Eds D. Caldwell, E., J. Brierley, A. and C. Brierley, L.), pp. 3-16. Van Nostrand REinhold Company, New York.

Grötsch, J., Suwaina, O., Ajlani, G., Taher, A., El-Khassawneh, R., Lokier, S., Coy, G., van der Weerd, E., Masalmeh, S. and van Dorp, J. (2003) The Arab Formation in central Abu Dhabi: 3-D reservoir architecture and static and dynamic modeling. *GeoArabia*, **8,** 47-86.

Höhn, A., Tobschall, H.J. and Maddock, J.E.L. (1986) Biogeochemistry of a hypersaline lagoon east of Rio de Janeiro, Brazil. *Science of the Total Environment*, **58,** 175-185.

Jahnert, R.J. and Collins, L.B. (2011) Significance of subtidal microbial deposits in Shark Bay, Australia. *Marine Geology*, **286,** 106-111.

Jahnert, R.J. and Collins, L.B. (2013) Controls on microbial activity and tidal flat evolution in Shark Bay, Western Australia. *Sedimentology*, **60,** 1071-1099.

Jordan, N., Allison, P.A., Hill, J. and Sutton, M.D. (2015) Not all aragonitic molluscs are missing: taphonomy and significance of a unique shelly lagerstätte from the Jurassic of SW Britain. *Lethaia*, **48,** 540-548.

Kendall, C.G.S.C. and Skipwith, P.A.D.E. (1968) Recent algal mats of a Persian Gulf Lagoon. *Journal of Sedimentary Petrology*, **38,** 1040-1058.

Kendall, C.G.S.C. and Skipwith, P.A.D.E. (1969) Holocene shallow-water carbonate and evaporite sediments of Khor al Bazam, Abu Dhabi, Southwest Persian Gulf. *AAPG Bulletin*, **53,** 841-869.

Kenig, F., Huc, A.Y., Purser, B.H. and Oudin, J.L. (1990) Sedimentation, distribution and diagenesis of organic-matter in a recent carbonate environment, Abu-Dhabi, UAE. *Organic Geochemistry*, **16,** 735-747.

Lambeck, K. (1996) Shoreline reconstructions for the Persian Gulf since the last glacial maximum. *Earth and Planetary Science Letters*, **142,** 43-57.

Logan, B.W. (1961) Cryptozoon and Associate Stromatolites from the Recent, Shark Bay, Western Australia. *The Journal of Geology*, **69,** 517-533.

Logan, B.W., Hoffman, P. and Gebelein, C.D. (1974) Algal Mats, Cryptalgal Fabrics, and Structures, Hamelin Pool, Western Australia. In: *Memoir 22: Evolution and Diagenesis of Quaternary Carbonate Sequences, Shark Bay, Western Australia*, pp. 140-194. American Association of Petroleum Geologists, Tulsa, Arizona.

Lokier, S. and Steuber, T. (2008) Quantification of carbonate-ramp sedimentation and progradation rates for the late Holocene Abu Dhabi shoreline. *Journal of Sedimentary Research*, **78,** 423-431.

Lokier, S. and Steuber, T. (2009) Large-scale intertidal polygonal features of the Abu Dhabi coastline. *Sedimentology*, **56,** 609-621.

Lokier, S.W. (2012) Development and evolution of subaerial halite crust morphologies in a coastal sabkha setting. *Journal of Arid Environments*, **79,** 32-47.

Lokier, S.W., Andrade, L.L., Court, W.M., Dutton, K.E., Head, I.M., van der Land, C., Paul, A. and Sherry, A. (2017) A new model for the formation of microbial polygons in a coastal sabkha setting. *The Depositional Record*, **3,** 201-208.

Lokier, S.W., Bateman, M.D., Larkin, N.R., Rye, P. and Stewart, J.R. (2015) Late Quaternary sea-level changes of the Persian Gulf. *Quaternary Research*, **84,** 69-81.

Lokier, S.W., Court, W.M., Onuma, T. and Paul, A. (2018) Implications of sea-level rise in a modern carbonate ramp setting. *Geomorphology*, **304,** 64-73.

Lovelock, C.E., Cahoon, D.R., Friess, D.A., Guntenspergen, G.R., Krauss, K.W., Reef, R., Rogers, K., Saunders, M.L., Sidik, F., Swales, A., Saintilan, N., Thuyen, L.X. and Triet, T. (2015) The vulnerability of Indo-Pacific mangrove forests to sea-level rise. *Nature*, **526,** 559-563.

Monty, C.L.V. (1972) Recent algal stromatolitic deposits, Andros Island, Bahamas. Preliminary report. *Geologische Rundschau*, **61,** 742-783.

Oliveri, E., Neri, R., Bellanca, A. and Riding, R. (2010) Carbonate stromatolites from a Messinian hypersaline setting in the Caltanissetta Basin, Sicily: petrographic evidence of microbial activity and related stable isotope and rare earth element signatures. *Sedimentology*, **57,** 142-161.

Özkul, M., Gökgöz, A., Kele, S., Baykara, M.O., Shen, C.C., Chang, Y.W., Kaya, A., Hançer, M., Aratman, C., Akin, T. and Örü, Z. (2014) Sedimentological and geochemical characteristics of a fluvial travertine: A case from the eastern Mediterranean region. *Sedimentology*, **61,** 291-318.

Paul, A. and Lokier, S.W. (2017) Holocene marine hardground formation in the Arabian Gulf: Shoreline stabilisation, sea level and early diagenesis in the coastal sabkha of Abu Dhabi. *Sedimentary Geology*, **352,** 1-13.

Perry, C.T., Alvarez-Filip, L., Graham, N.A.J., Mumby, P.J., Wilson, S.K., Kench, P.S., Manzello, D.P., Morgan, K.M., Slangen, A.B.A., Thomson, D.P., Januchowski-Hartley, F., Smithers, S.G., Steneck, R.S., Carlton, R., Edinger, E.N., Enochs, I.C., Estrada-Saldívar, N., Haywood, M.D.E., Kolodziej, G., Murphy, G.N., Pérez-Cervantes, E., Suchley, A., Valentino, L., Boenish, R., Wilson, M. and Macdonald, C. (2018) Loss of coral reef growth capacity to track future increases in sea level. *Nature*, **558,** 396.

Petrash, D.A., Bialik, O.M., Bontognali, T.R.R., Vasconcelos, C., Roberts, J.A., McKenzie, J.A. and Konhauser, K.O. (2017) Microbially catalyzed dolomite formation: From near-surface to burial. *Earth-Science Reviews*, **171,** 558-582.

Raafat, H. (2007) Climate. In: *Physical Geography Sector Paper* (Ed A. Kumar), pp. 72-89. Environment Agency Abu Dhabi.

Reid, P.R., James, N.P., Macintyre, I.G., Dupraz, C.P. and Burne, R.V. (2003) Shark Bay stromatolites: Microfabrics and reinterpretation of origins. *Facies*, **49,** 299.

Riding, R. (1999) The term stromatolite: towards an essential definition. *Lethaia***,** 321-330.
Sandberg, P., Schneidermann, N. and Harris, P.M. (1985) Aragonite Cements and their Occurrence in Ancient Limestones. In: *Carbonate Cements: Based on a Symposium Sponsored by the Society of Economic Paleontologists and Mineralogists*, **36**, pp. 0. SEPM Society for Sedimentary Geology.
Shinn, E.A. (1969) Submarine lithification of Holocene carbonate sediments in the Persian Gulf. *Sedimentology*, **12,** 109-144.
Stolz, J.F., Reid, R.P., Visscher, P.T., Decho, A.W., Norman, R.S., Aspden, R.J., Bowlin, E.M., Franks, J., Foster, J.S., Paterson, D.M., Przekop, K.M., Underwood, G.J.C. and Prufert-Bebout, L. (2009) The microbial communities of the modern marine stromatolites at Highborne Cay, Bahamas. *Atoll Research Bulletin*, **567,** 1-29.
Suosaari, E.P., Reid, R.P., Araujo, T.A.A., Playford, P.E., Holley, D.K., McNamara, K.J. and Eberli, G.P. (2016a) Environmental Pressures Influencing Living Stromatolites in Hamelin Pool, Shark Bay, Western Australia. *PALAIOS*, **31,** 483-496.
Suosaari, E.P., Reid, R.P., Playford, P.E., Foster, J.S., Stolz, J.F., Casaburi, G., Hagan, P.D., Chirayath, V., Macintyre, I.G., Planavsky, N.J. and Eberli, G.P. (2016b) New multi-scale perspectives on the stromatolites of Shark Bay, Western Australia. *Scientific Reports*, **6,** 20557.
Thorner, J., Kumar, L. and Smith, S.D.A. (2014) Impacts of climate-change-driven sea level rise on intertidal rocky reef habitats will be variable and site specific. *PloS one*, **9,** e86130-e86130.
Trembath-Reichert, E., Ward, L.M., Slotznick, S.P., Bachtel, S.L., Kerans, C., Grotzinger, J.P. and Fischer, W.W. (2016) Gene Sequencing-Based Analysis of Microbial-Mat Morphotypes, Caicos Platform, British West Indies. *Journal of Sedimentary Research*, **86,** 629-636.
Vasconcelos, C., Warthmann, R., McKenzie, J.A., Visscher, P.T., Bittermann, A.G. and van Lith, Y. (2006) Lithifying microbial mats in Lagoa Vermelha, Brazil modern Precambrian relics? *Sedimentary Geology*, **185,** 175-183.
Wood, W.W. and Sanford, W.E. (2002) Hydrology and solute chemistry of coastal-sabkha aquifer in the Emirate of Abu Dhabi. In: *Sabkha Ecosystems, v. 1 - The Sabkhas of the Arabian Peninsula and Adjacent Countries* (Ed H.J.B. Barth, B.), pp. 173-185. Kluwer Academic Publishers.

Table and figure captions

Table 1. Environmental data from a range of coastal marine stromatolite and microbial mat provinces. Sources for the data: Sabkha: this study and studies given in local settings. Hamelin Pool: Water temperatures, salinity, tidal regime and tidal range from (Suosaari et al., 2016a), air temperatures, mean annual rainfall and wind speed from http://www.bom.gov.au; evaporation from Logan (1961). Lagoa Vermelha: Höhn et al. (1986). Cayo Coco: Bouton et al. (2016). Highborne Cay: Bowlin et al. (2012).

Figure 1. A) Location of the study area in relation to the Gulf. B) Location of study area in the context of the Abu Dhabi coastline. C) Satellite image of the coastal sabkha of Abu Dhabi, showing facies belts and anthropogenic changes. The study site is indicated by a white star. Imagery source: ESA Sentinel 2A Multi-spectral Imager (MSI), date: 18 March 2017.

Figure 2. A) Mean daily air temperatures in the coastal sabkha measured between February 2016 and June 2017 using a barometric logger (black line) and the GP1 weather station (red line). Daily maximum and daily minimum temperatures are shown in the background. Precipitation in January and February 2017 is indicated by the blue columns. B) Record of water temperatures and water depth in the studied intertidal pool, showing the daily tidal regime as well as long term annual trends in water depth. Note that the pool was never empty. C) Wind rose showing the dominant wind directions from the WNW - NW and S, and wind speeds. D) Frequency distribution plots of wind speeds for two intervals in January – February 2017 and in July – August 2016. Each vertical bar represents a 0.5 m/s wind speed interval.

Figure 3. A) Overview photograph of the studied pool. Note that the scale is not uniform from bottom to top due to the mode of image acquisition; person in background is 175 cm high. B) Interpretative overview of the features observed in the pool. Seaward direction is to the left. Note the detached bands at the pool margins, and the thrombolites towards the centre of the pool. C) Schematic cross-section through the pool showing the general stratigraphy, lithologies and features described in this study.

Figure 4. A) Close-up view of the lithified sill – see Fig. 3 for image location in the studied pool. The ephemeral pond system is located at the top of the image, while the pool is towards the bottom (not visible). The location of the water level logger is indicated by an arrow. Note the colonisation of the logger by cyanobacteria and algae. B) Schematic cross-section showing with the relationship between the ephemeral pond system, lithified sill and the pool.

Figure 5. A) Photograph of the organic ooze covering parts of the pool floor. Grazing trails of gastropods are visible with the respective gastropods at the end-points (arrows). B) Close-up view of the ooze and a gastropod (large arrow) and its grazing trail (small arrows).

Figure 6. A) Microbial 'gravel' collected from the pool floor. Different colours correspond to different organic pigments. B-D) Close-up views of individual microbial grains showing the EPS and white bioclastic grains embedded (arrow).

Figure 7. A) Close-up view of different microbial structures including thrombolites and stromatolites. Note the detached rim and the domal and banded thrombolites, surrounded by organic ooze and gravel-sized grains of microbial origin. Note also the aluminium can overgrown by microbial communities and partially covered by organic ooze. B) Close-up

view of an individual thrombolite showing its components: brown thrombolite, bioclasts and algae growth. Upper growth boundary of these algae indicates the minimum water depth in the pool, which corresponds to a depth of ~20 cm as also calculated from the water level logger data. See Fig. 3 for image location in the studied pool.

Figure 8. A) Cross-sectional view of an individual domal thrombolite, showing a clotted texture with internal crude radial laminations, based on differences in colour. Bioclasts enclosed by microbial EPS indicate outward growth. Coarse laminae are indicated by dashed lines. B) Hand specimen of a stromatolite from the pool margin. Microbial laminations preserved through lithification are clearly visible (between white arrows). Purple and green colours correspond to pigments of living cyanobacterial communities and are unrelated to the primary processes that lead to the development of the stromatolite.

Figure 9. Oblique subaqueous view of the partially undercut margin at the north-west side of the pool - see Fig. 3 for image location in the studied pool. Note the laminated stromatolites at the centre (white arrow).

Figure 10. Overview photograph showing the transition from the pool, via a rim overgrown with algae, into the surrounding polygonal microbial mat zone. Note that the polygonal microbial mat in the transition zone appears to be degraded. See Fig. 3 for image location in relation to the studied pool.

Figure 11. A) An area of recently eroded microbial mat exposing the underlying unconsolidated sediment. Note the incoming tide in the bottom left of the image (person is 185 cm tall). B) An erosive scour in the microbial mat zone. C) Schematic cross-section through the scour.

Figure 12. Thin section photomicrographs of stromatolites and thrombolites from the pool margin. A) Lithoclasts embedded in a stromatolite are shown surrounded by microbial organic-rich rims (arrow). B) Mouldic porosity in a thrombolitic area filled by acicular aragonite cements (arrows). C, D) Acicular aragonite cements filling thrombolite intragranular pore space. E, F) Discontinuous organic seams define the microbial laminations observed in hand specimen (see Fig. 8B) (arrows).

Figure 13. Scanning electron microscope micrographs of stromatolites and thrombolites. A, B) Extra-polymeric bacterial substance covering some areas of stromatolite specimen from the pool margin. Note bacterial filaments (white arrows). C) Crystal showing a very high Mg content indicative of proto-dolomite (arrow). The crystal is surrounded by aragonite cement and microbial EPS. D) Group of proto-dolomite crystals with very high Mg contents, surrounded by bacterial filaments, EPS and aragonite. E) Mineral precipitates in the microbialites showing cyanobacterial tubes (arrows). F) Acicular aragonite covered by a layer of EPS (arrows).

Figure 14. Schematic model of pool and microbial feature formation in the coastal sabkha of Abu Dhabi. A) Stratigraphy in the polygonal microbial mat zone prior to pool formation. B) Newly-formed pool with cyanobacteria colonising newly-formed subaqueous environments. C) Cementation of pool wall with onset of erosion. D) Pool margin collapse and formation of margin-parallel thrombolite band. E) Onset of new phase of pool wall cementation, continued growth of thrombolite, renewed erosion. F) Second generation of margin collapse, increasing isolation of phase 1 thrombolite.

Figure 15. Schematic overview of the process that leads to permanent water coverage of the pool. During highest tides the pool is inundated by ~ 1m of water. During low tide the ephemeral ponds system slowly empties its excess water into the pool. Since this process takes much longer than one tidal cycle, the pool remains filled with water. At the margin, cascading water results in degassing, promoting the precipitation of aragonite cements. (MHW = mean high water)

	Location				
Parameter	**Sabkha**	**Hamelin Pool**	**Lagoa Vermelha**	**Cayo Coco**	**Highborne Cay**
Air temperature (°C)	8.4 – 53.7	9.2 – 36.9	17.0 – 32.0	20.0 – 32.5	-
Water temperature (°C)	11.7 – 46.8	11.0 – 33.0	23.8 – 36.5	28.0 – 30.0	20.3 – 30.3
Salinity (‰)	75.0 – 93.0	15.8 – 88.1	40 – 84	30 – 80	35
Mean annual rainfall (mm)	72.0	210.4	900	1000	-
Annual evaporation (mm)	2750	2032 - 2286	1300	2100 – 2200	-
Tidal range (m)	1.0	1.0	1.0 – 1.7	0.3	1.0
Mean wind speed (m/s)	3.7	2.8	-	3.9	4.18

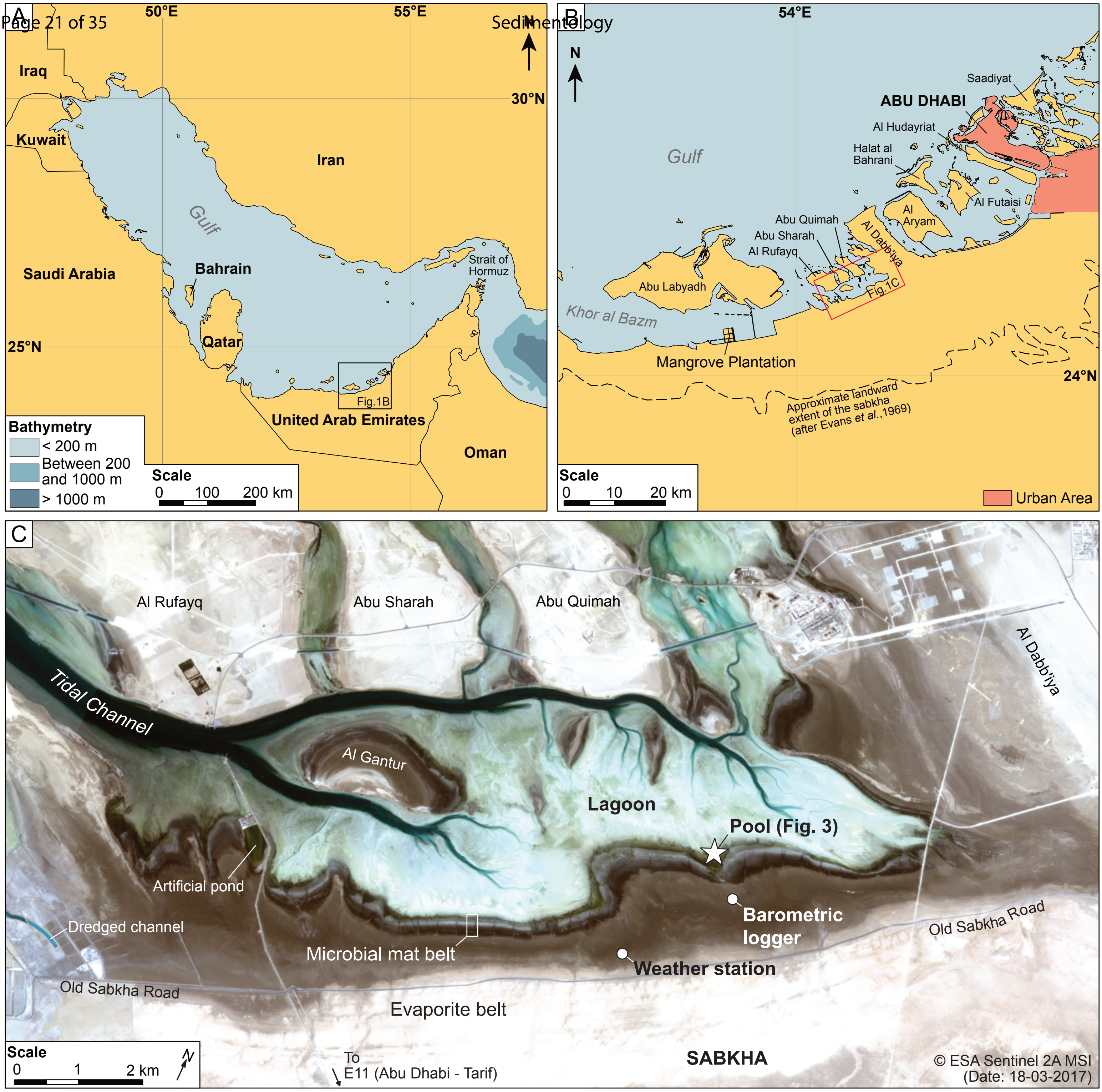
A
50°E
55°E
N
30°N
25°N
Iraq
Kuwait
Iran
Gulf
Saudi Arabia
Bahrain
Qatar
Strait of Hormuz
Fig.1B
United Arab Emirates
Oman
Bathymetry
< 200 m
Between 200 and 1000 m
> 1000 m
Scale
0 100 200 km
B
54°E
N
Gulf
Saadiyat
ABU DHABI
Al Hudayriat
Halat al Bahrani
Al Futaisi
Al Aryam
Abu Quimah
Abu Sharah
Al Rufayq
Al Dabbi'ya
Fig.1C
Abu Labyadh
Khor al Bazm
Mangrove Plantation
24°N
Approximate landward extent of the sabkha (after Evans et al.,1969)
Scale
0 10 20 km
Urban Area
C
Al Rufayq
Abu Sharah
Abu Quimah
Al Dabbi'ya
Tidal Channel
Al Gantur
Lagoon
Pool (Fig. 3)
Artificial pond
Dredged channel
Barometric logger
Microbial mat belt
Weather station
Old Sabkha Road
Old Sabkha Road
Evaporite belt
Scale
0 1 2 km
N
To E11 (Abu Dhabi - Tarif)
SABKHA
© ESA Sentinel 2A MSI (Date: 18-03-2017)

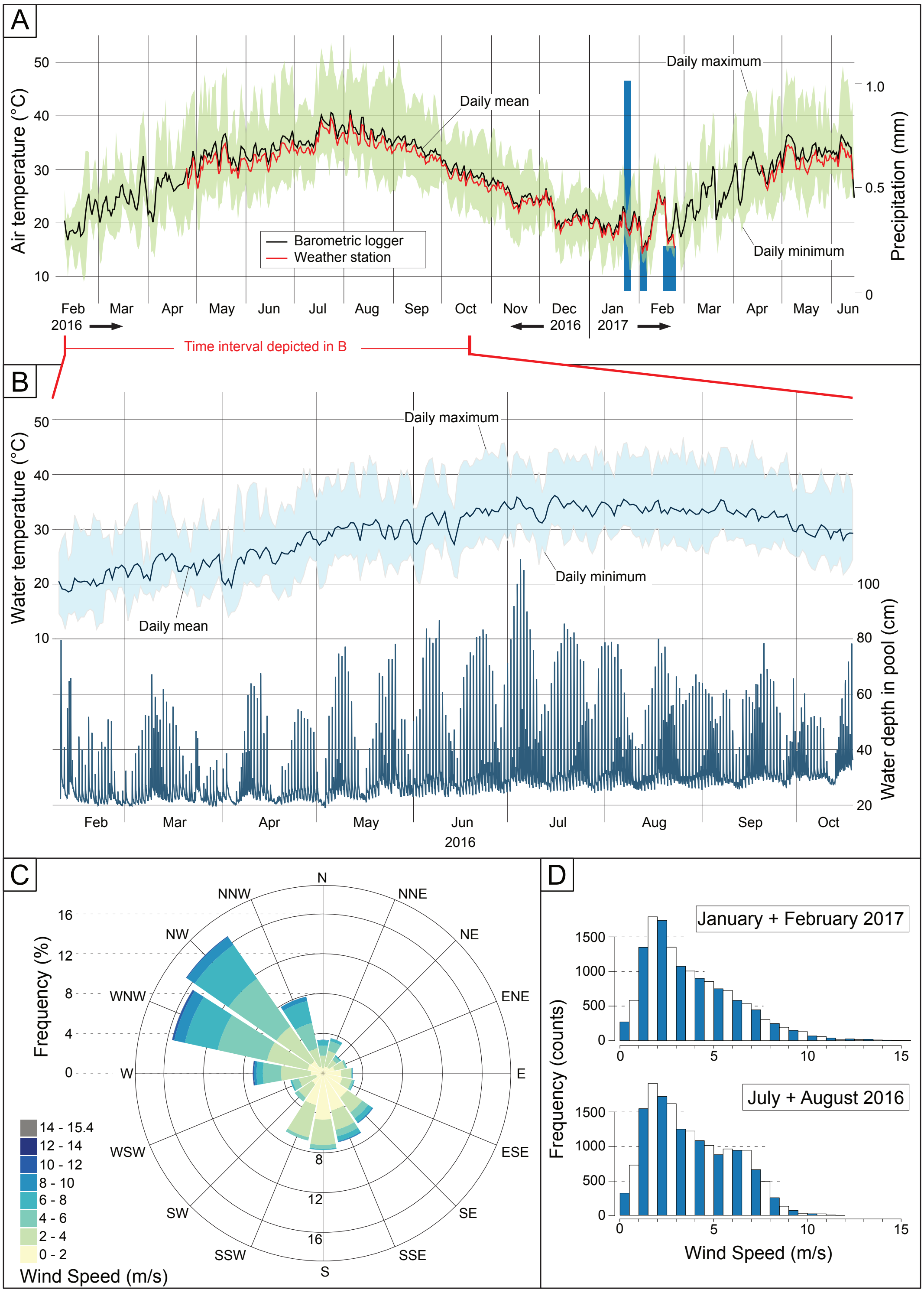
A
Air temperature (°C)
50
40
30
20
10
Daily maximum
Daily mean
Daily minimum
Barometric logger
Weather station
Precipitation (mm)
1.0
0.5
0
Feb
Mar
Apr
May
Jun
Jul
Aug
Sep
Oct
Nov
Dec
Jan
Feb
Mar
Apr
May
Jun
2016
2016
2017
Time interval depicted in B
B
Water temperature (°C)
Daily maximum
Daily minimum
Daily mean
Water depth in pool (cm)
100
80
60
40
20
Feb
Mar
Apr
May
Jun
Jul
Aug
Sep
Oct
2016
C
Frequency (%)
16
12
8
4
0
N
NNE
NE
ENE
E
ESE
SE
SSE
S
SSW
SW
WSW
W
WNW
NW
NNW
14 - 15.4
12 - 14
10 - 12
8 - 10
6 - 8
4 - 6
2 - 4
0 - 2
Wind Speed (m/s)
D
Frequency (counts)
January + February 2017
July + August 2016
1500
1000
500
0
0
5
10
15
Wind Speed (m/s)

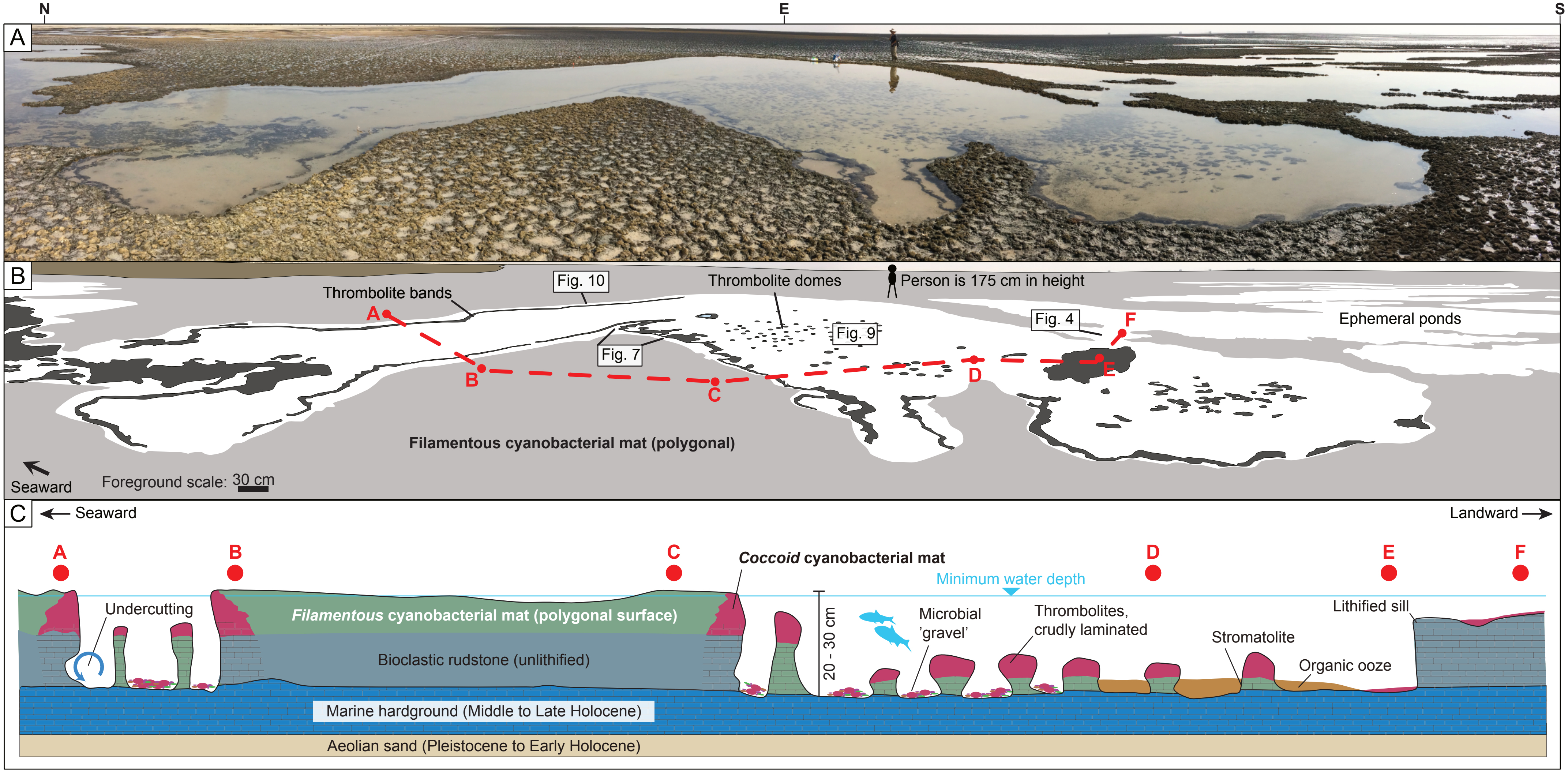
N
E
S
A
B
Thrombolite bands
Fig. 10
Thrombolite domes
Person is 175 cm in height
Fig. 4
Ephemeral ponds
Fig. 9
Fig. 7
A
B
C
D
E
F
Filamentous cyanobacterial mat (polygonal)
Seaward
Foreground scale: 30 cm
C
Seaward
Landward
A
B
C
D
E
F
Coccoid cyanobacterial mat
Minimum water depth
Undercutting
Filamentous cyanobacterial mat (polygonal surface)
Bioclastic rudstone (unlithified)
20 - 30 cm
Microbial 'gravel'
Thrombolites, crudly laminated
Lithified sill
Stromatolite
Organic ooze
Marine hardground (Middle to Late Holocene)
Aeolian sand (Pleistocene to Early Holocene)

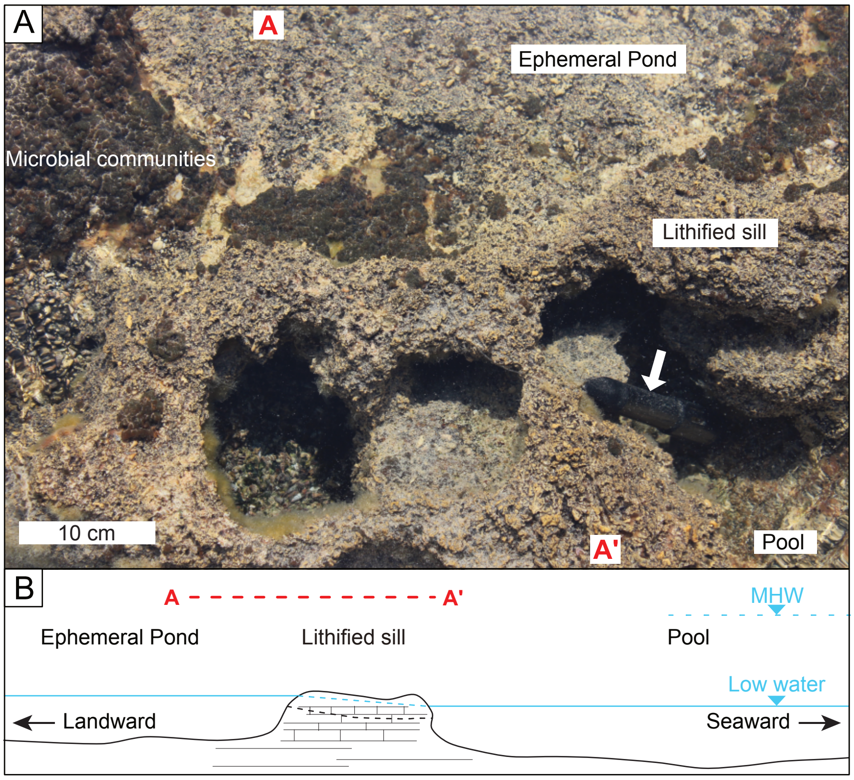
A
A
Ephemeral Pond
Microbial communities
Lithified sill
10 cm
A'
Pool
B
A - - - - - - - - - - - - A'
MHW
Ephemeral Pond
Lithified sill
Pool
Low water
Landward
Seaward

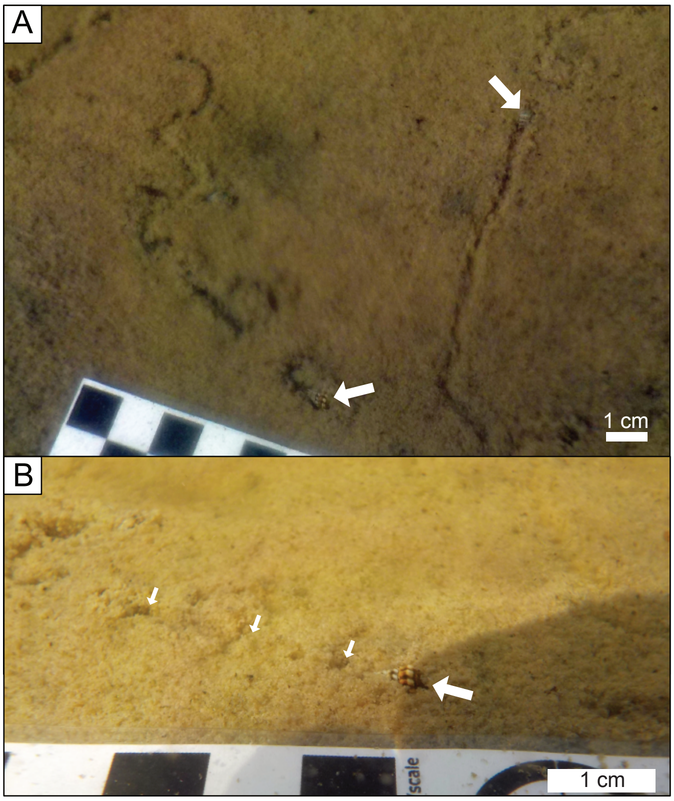
A
1 cm
B
scale
1 cm

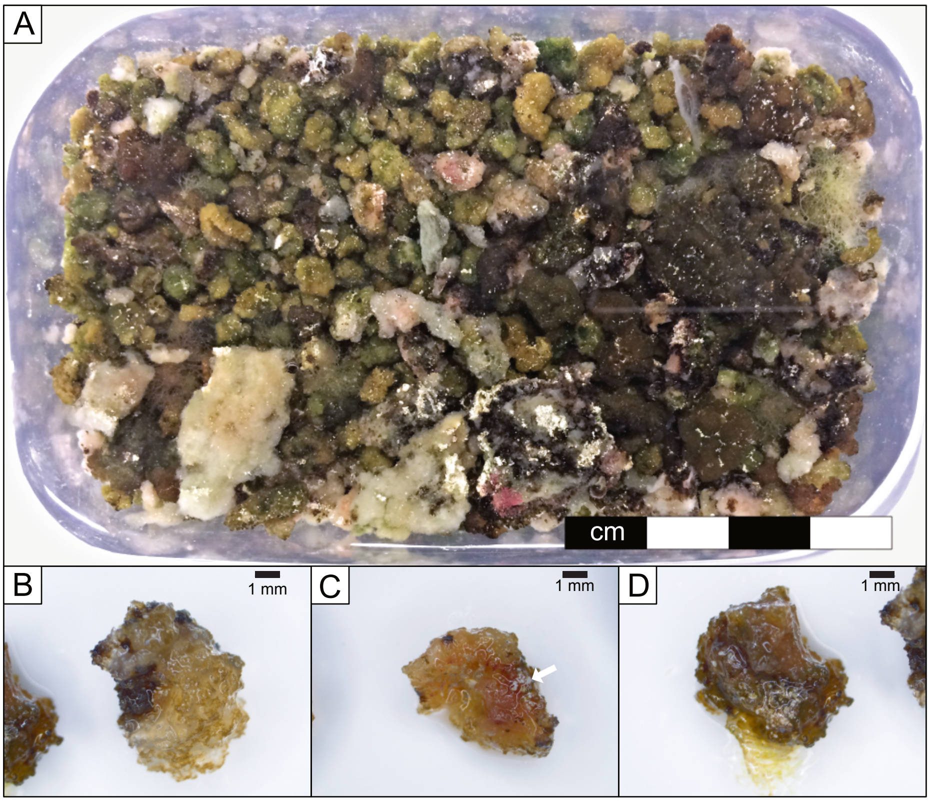
A
cm
B
1 mm
C
1 mm
D
1 mm

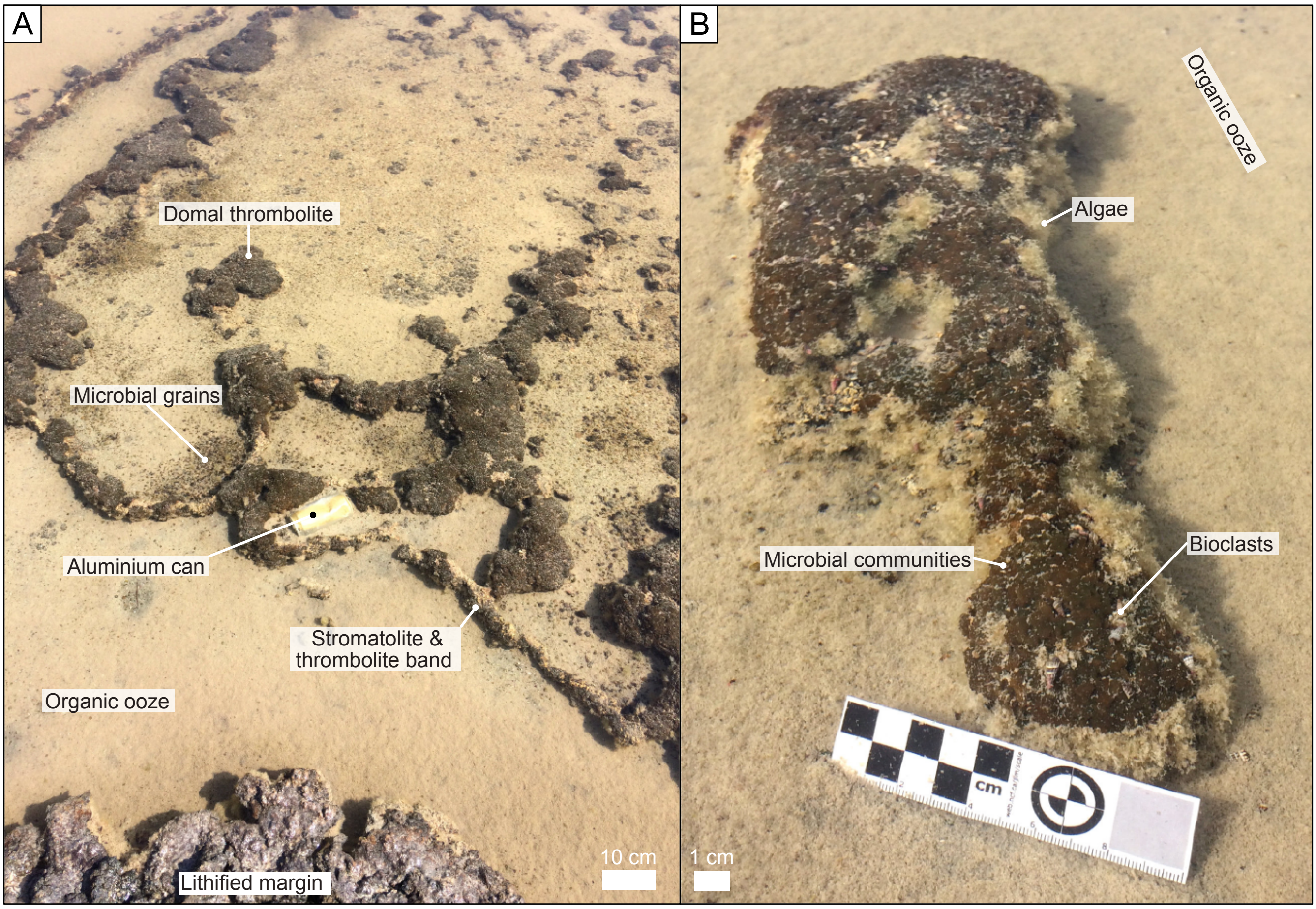
A
Domal thrombolite
Microbial grains
Aluminium can
Stromatolite & thrombolite band
Organic ooze
Lithified margin
10 cm
B
Organic ooze
Algae
Microbial communities
Bioclasts
1 cm
cm

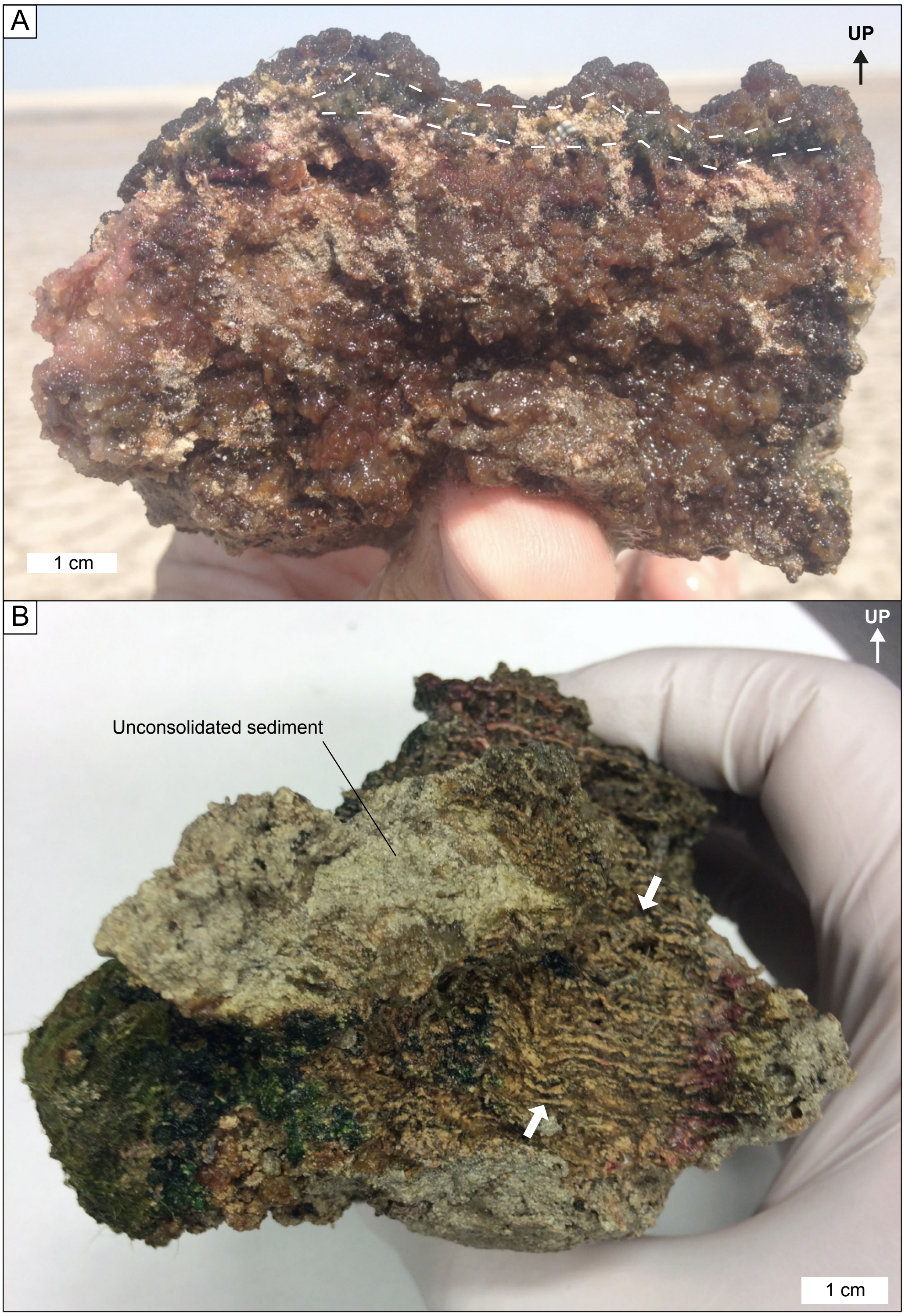
A
UP
1 cm
B
UP
Unconsolidated sediment
1 cm

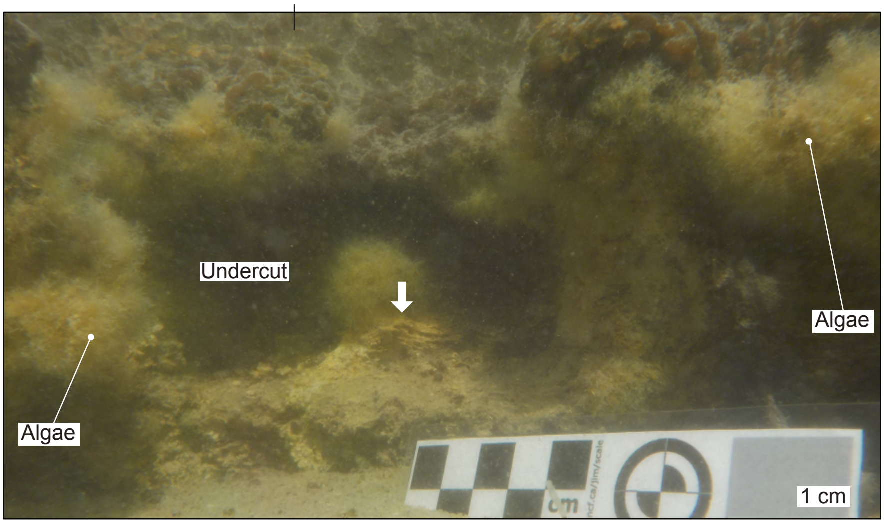
Pustular microbial communities
Undercut
Algae
Algae
1 cm

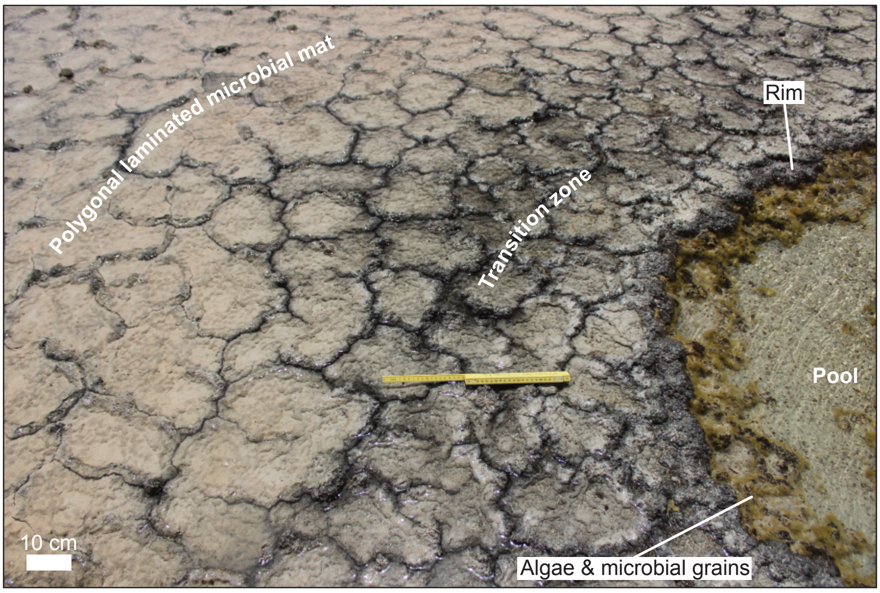
Polygonal laminated microbial mat
Transition zone
Rim
Pool
10 cm
Algae & microbial grains

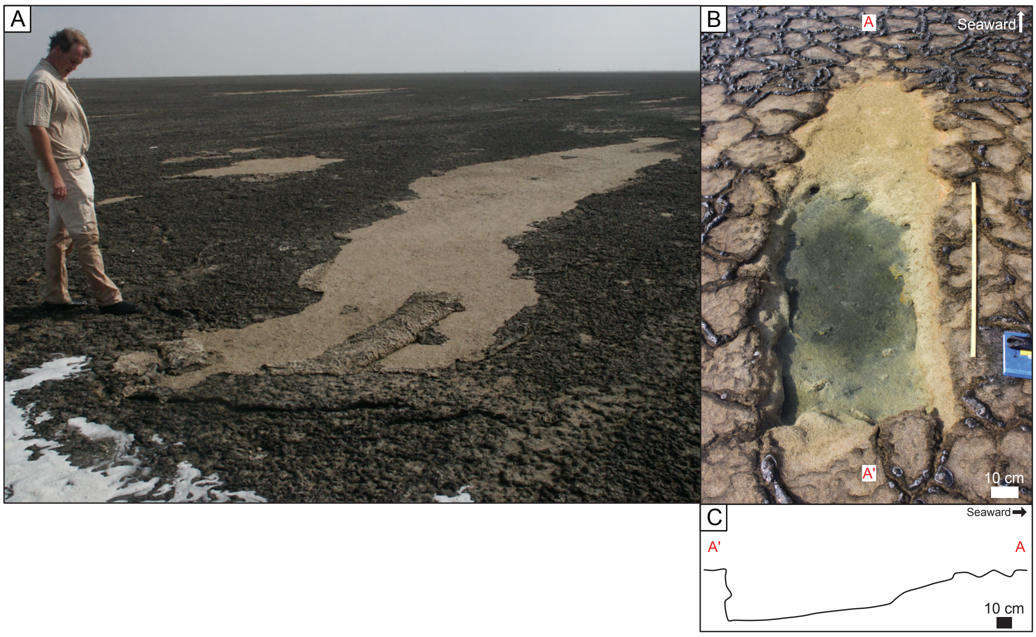
A
B
A
Seaward
A'
10 cm
C
Seaward
A'
A
10 cm

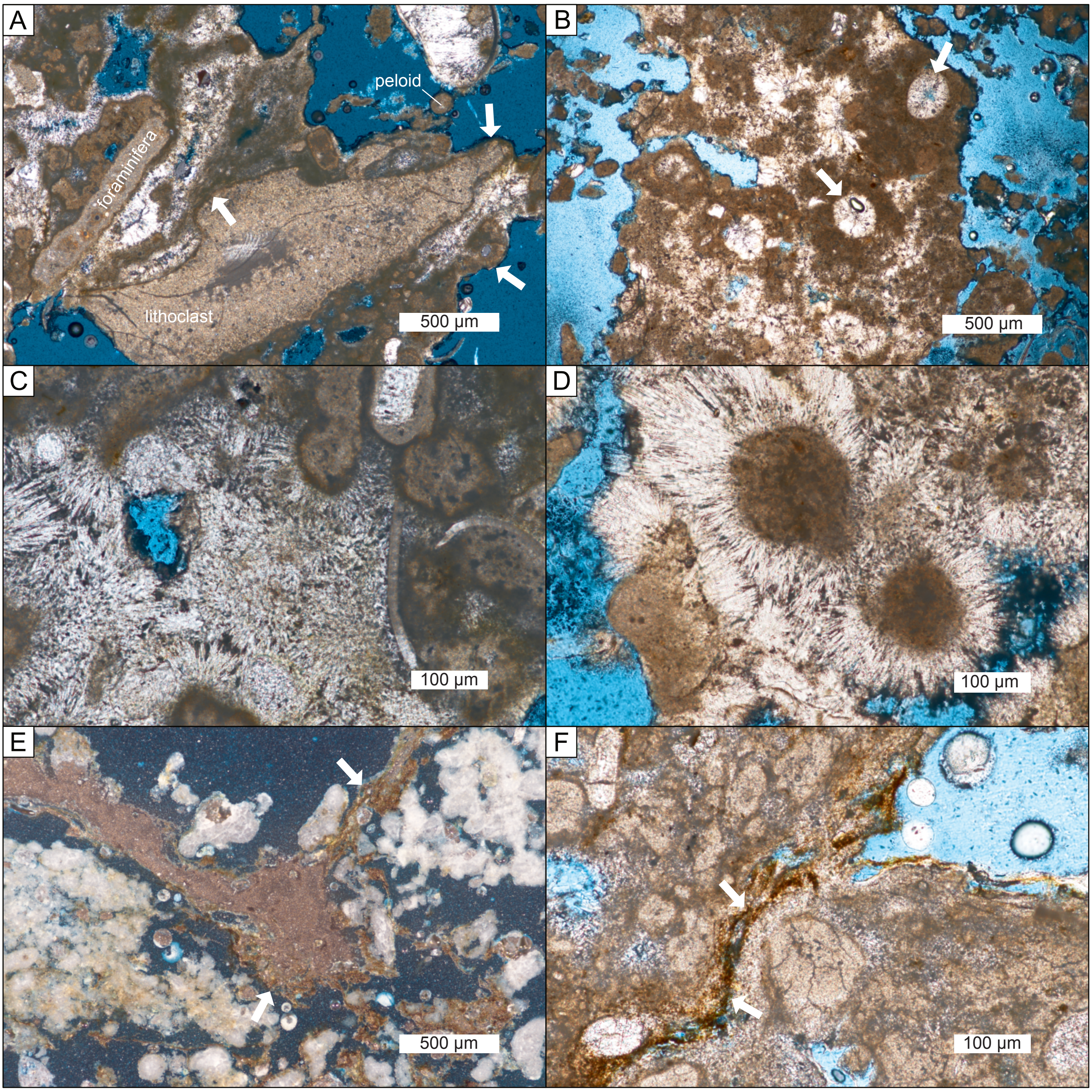
A
peloid
foraminifera
lithoclast
500 µm
B
500 µm
C
100 µm
D
100 µm
E
500 µm
F
100 µm

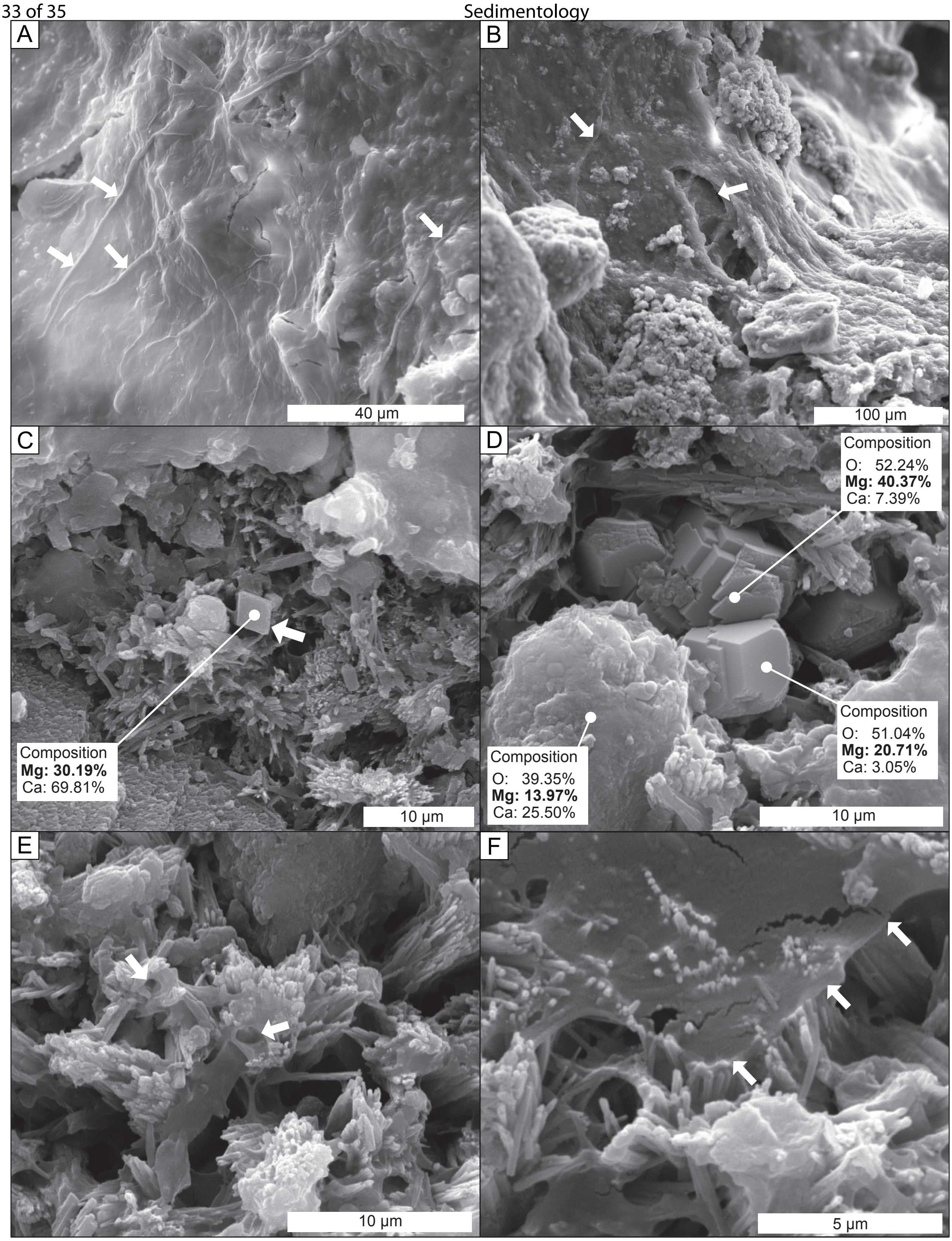
A
40 µm
B
100 µm
C
Composition
Mg: 30.19%
Ca: 69.81%
10 µm
D
Composition
O: 52.24%
Mg: 40.37%
Ca: 7.39%
Composition
O: 51.04%
Mg: 20.71%
Ca: 3.05%
Composition
O: 39.35%
Mg: 13.97%
Ca: 25.50%
10 µm
E
10 µm
F
5 µm

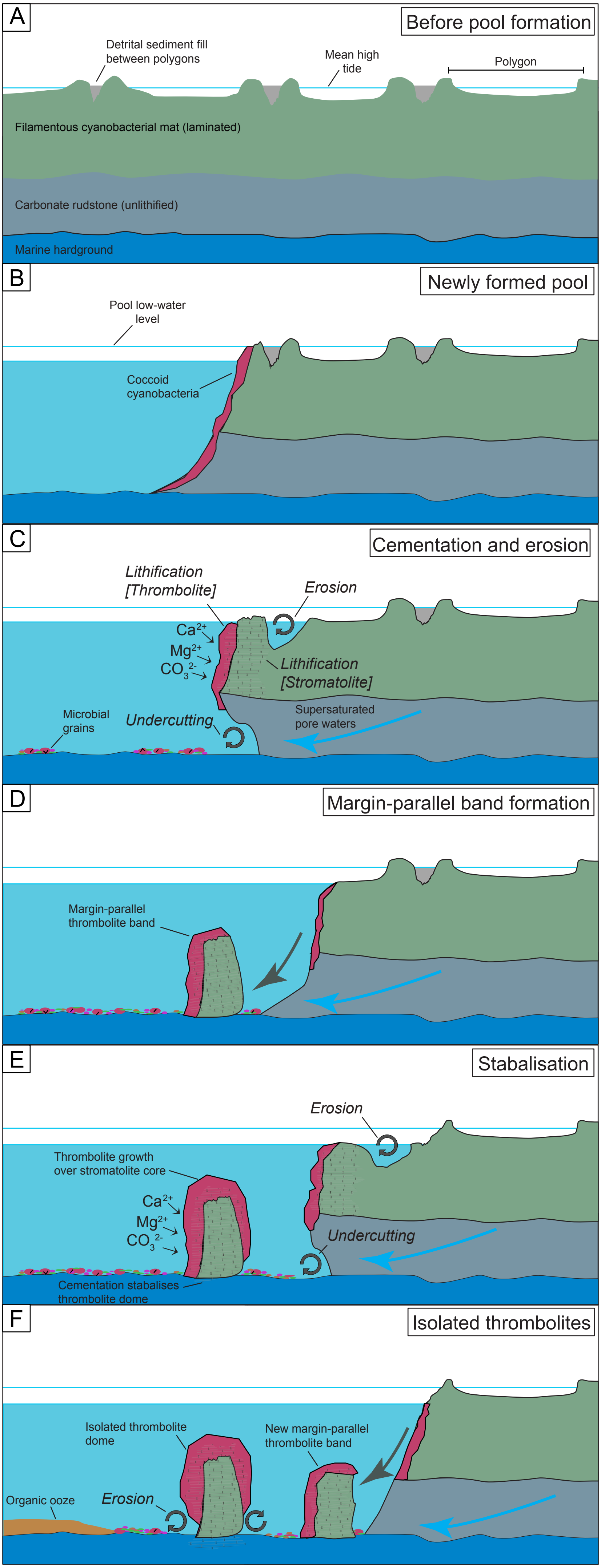
A
Before pool formation
Detrital sediment fill between polygons
Mean high tide
Polygon
Filamentous cyanobacterial mat (laminated)
Carbonate rudstone (unlithified)
Marine hardground
B
Newly formed pool
Pool low-water level
Coccoid cyanobacteria
C
Cementation and erosion
Lithification [Thrombolite]
Erosion
Ca^{2+}
Mg^{2+}
CO_3^{2-}
Lithification [Stromatolite]
Microbial grains
Undercutting
Supersaturated pore waters
D
Margin-parallel band formation
Margin-parallel thrombolite band
E
Stabalisation
Erosion
Thrombolite growth over stromatolite core
Ca^{2+}
Mg^{2+}
CO_3^{2-}
Undercutting
Cementation stabalises thrombolite dome
F
Isolated thrombolites
Isolated thrombolite dome
New margin-parallel thrombolite band
Organic ooze
Erosion

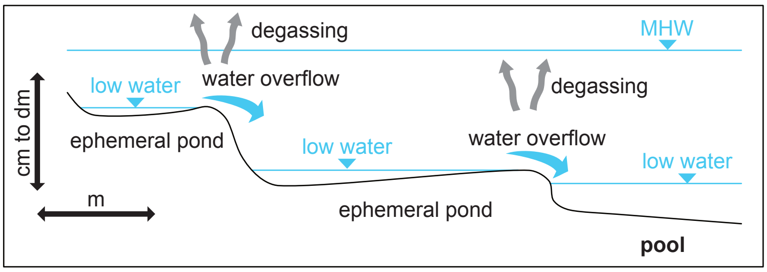
degassing
MHW
low water
water overflow
degassing
cm to dm
ephemeral pond
low water
water overflow
low water
m
ephemeral pond
pool